Comparison of the corrosion resistance of AA2024 and AA2098 alloys in different solutions

Mariana X. MILAGRE[1], João Victor de Sousa ARAUJO[2], Maurilio Pereira GOMES[3], Uyime Donatus[4], Caruline S.C. MACHADO[5], Isolda COSTA[6]

[1]Instituto de Pesquisas Energéticas e Nucleares, Centro de Ciência e Tecnologia de Materiais, São Paulo, Brazil, marianamiagre@yahoo.com.br
[2]Instituto de Pesquisas Energéticas e Nucleares, Centro de Ciência e Tecnologia de Materiais, São Paulo, Brazil, joao-neutron@hotmail.com
[3]Instituto de Pesquisas Energéticas e Nucleares, Centro de Ciência e Tecnologia de Materiais, São Paulo, Brazil, Maurilio Gomes maurilio.pereira.gomes@gmail.com
[4]Instituto de Pesquisas Energéticas e Nucleares, Centro de Ciência e Tecnologia de Materiais, São Paulo, Brazil, uymedonatus@yahoo.com
[5]Instituto de Pesquisas Energéticas e Nucleares, Centro de Ciência e Tecnologia de Materiais, São Paulo, Brazil, carulinemachado@yahoo.com.br
[6]Instituto de Pesquisas Energéticas e Nucleares, Centro de Ciência e Tecnologia de Materiais, São Paulo, Brazil, icosta@ipen.br

Abstract

In this work the corrosion resistance of the AA2098-T351 and AA2024-T3 was evaluated and compared by electrochemical tests in 0.01 mol.L^{-1} of NaCl and 0.1 mol.L^{-1} of Na_2SO_4 with 0.001 mol.L^{-1} NaCl electrolytes. Monitoring of corrosion evolution in both alloys was carried out by electrochemical impedance spectroscopy (EIS) and polarization methods. The surface of the samples exposed to the test solutions was observed by microscopy after corrosion tests. The results showed different corrosion mechanisms in the two test solutions. In the sulfate containing electrolyte, the Al-Cu-Li alloy showed corrosion mechanism mainly associated with the micrometric particles at the surface, similarly to the AA2024-T3 alloy. However, in the chloride solution without sulfate, the AA2098-T351 alloy showed susceptibility to severe localized corrosion (SLC) besides the corrosion associated to the micrometric particles and the first type of corrosion was the main type of attack. The AA2024-T3 showed lower susceptibility to SLC than the AA2098-T351 alloy.

Key-words: localized corrosion; electrochemical impedance spectroscopy; polarization curves

Introduction

The aluminum-copper-lithium (Al-Cu-Li) alloys were developed as potential replacements for the conventional aluminum-copper (Al-Cu) alloys from the 2XXX series for applications in aircraft industry [1–3]. Additions of lithium lead to increase in specific strength (E/ρ) without toughness loss [4]. Thus, an economy in fuel is achieved. However, lithium is a highly reactive element and its addition to the alloys affects their corrosion resistance [5–10].

Aluminum alloys are susceptible to various types of localized corrosion, such as pitting, intergranular corrosion (IGC) and stress corrosion cracking (SCC) [11–16]. The corrosion mechanism of aluminum alloys in chloride media has been previously reported [14-16]. According to McCafferty [15,16] pitting initiates by adsorption of chloride ions over the oxide layer surface; subsequently these ions penetrate through the defects in the oxide layer and; at last, localized dissolution of aluminum occurs in the metal/oxide interface. The localized corrosion rate is controlled by the solution composition inside the pit, that is, controlled by diffusion [14].

The corrosion behavior of conventional aluminum alloys is well known [17–23]. For instance, for the AA2024 alloy corrosion is mainly associated with the selective dissolution of Al_2CuMg, S phase. This phase is initially anodic in relation to the matrix. After preferential magnesium dissolution, the attack starts in the surrounding matrix and in the precipitate free zones (PFZ) at the grain boundaries [24]. Moreover, the process of Al and Mg dissolution lead to Cu re-deposition at the passive film that changes the film properties and favors susceptibility to localized corrosion [11].

The corrosion susceptibility of Al-Cu-Li alloys has been largely reported [5,8,10,25–27]. Despite the corrosion associated with the cathodic micrometric particles, the major mechanism is associated with the nanometric T1 phase (Al_2CuLi) [8,10,28,29]. This type of corrosion is known as severe localized corrosion (SLC) and is characterized by rings of corrosion products surrounding the anodic sites and hydrogen gas evolution at the active sites [26,27].

Conde and Damborenea [30] used electrochemical impedance spectroscopy (EIS) in chloride containing solutions to investigate the corrosion resistance of Aluminum alloys and showed that the process is controlled by activation in the first hours of immersion but diffusion controlled for long periods of test. Ryl *et al*.[31] showed that changes in the passive layer composition can improve the electrochemical properties of Al-alloys. Chen *et al.* [32] also used EIS techniques to report the influence of precipitates on the electrochemical properties of the passive film on the AA7075 alloy.

Despite the massive information on the electrochemical behavior of conventional aluminum alloys, such as AA2024-T3, the use of EIS for electrochemical characterization of Al-Cu-Li alloys is still scarce. Also, the effect of low aggressive environments on the corrosion resistance of these alloys has not been much reported [33–35]. In order to contribute with information about the electrochemical behavior of the AA2098-T351, an Al-Cu-Li alloy, in environment of low aggressiveness, its corrosion resistance was evaluated by electrochemical techniques in 0.01 $mol.L^{-1}$ NaCl and 0.1 $mol.L^{-1}$ Na_2SO_4 with 0.001 $mol.L^{-1}$ of Na solutions and compared with that of the AA2024-T3 alloy.

Experimental

The chemical composition of the alloys used in this study is shown in Table 1.

Table 1 - Chemical composition (wt%) obtained by Inductively Coupled Plasma-Atomic Emission Spectroscopy (ICP-AES) of the alloys used in this study.

Alloy/Element	Al	Cu	Li	Mg	Ag	Zr	Fe	Si	Zn	Mn
AA2024-T3	93.5	4.2	-	1.6	-	-	0.20	0.10	0.20	0.40
AA2098-T351	94.5	3.4	1.0	0.3	0.3	0.4	0.04	0.05	0.02	0.003

The electrochemical characterization of the AA2098-T351 and AA2024-T3 alloys was carried out using an AUTOLAB PGSTAT potentiostat controlled by NOVA 1.11 software. The tests were performed at room temperature using a three electrode-cell experimental setup with an $Ag/AgCl_{KCl(sat)}$ electrode as reference electrode, and a platinum wire as counter electrode. The exposed area of the working electrode was 1 cm^2. Anodic polarization curves were obtained from the open circuit potential (OCP) to 0.5 V vs. $Ag/AgCl_{KCl(sat)}$ and cathodic ones from OCP to -1.2 V vs. $Ag/AgCl_{KCl(sat)}$, both with a scan rate of 1 mV/s. EIS data were obtained potentiostatically at the OCP in the frequency range from 10 kHz to 10 mHz with 10 mV amplitude signal and acquisition rate of 10 points per decade. The electrolytes used in the electrochemical tests was 0.01 $mol.L^{-1}$ NaCl and 0.1 $mol.L^{-1}$ Na_2SO_4 with 0.001 $mol.L^{-1}$ NaCl solution at (22 ± 2) ^oC. Surface monitoring was carried out using optical microscopy and scanning electron microscopy (SEM) using a Hitachi TM 3000 microscope with an incident beam of 15 keV.

Results and Discussion

The variation of OCP for the tow alloys as a function of time of immersion in both test solutions are shown in Figure 1.

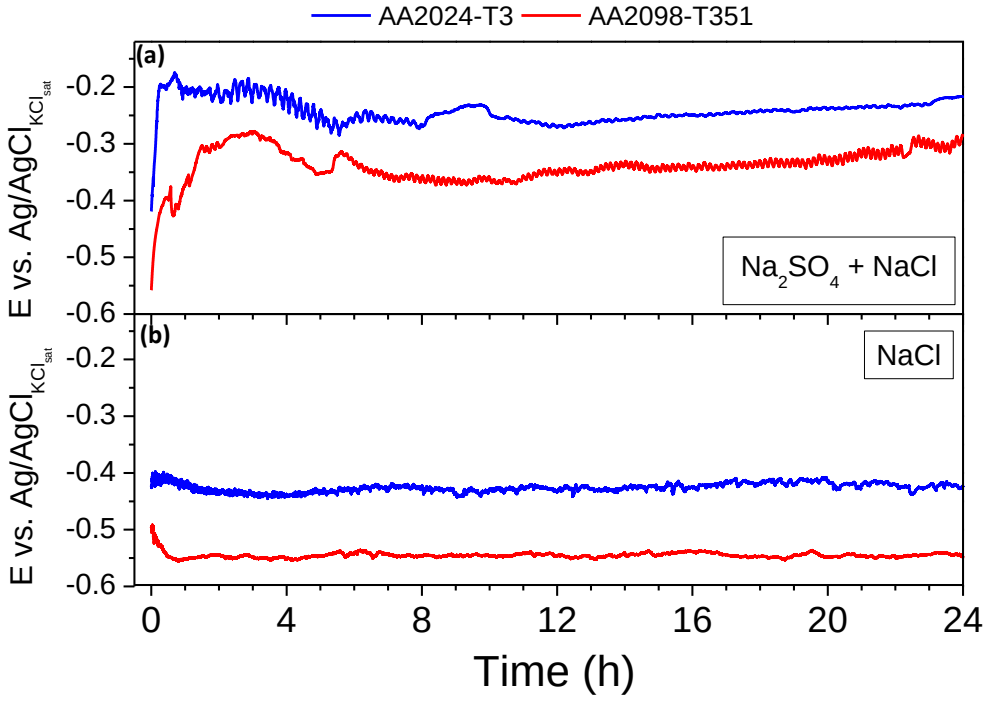

Figure 1 - Open circuit potential variation as a function of time of immersion for the AA2024-T3 and AA2098-T351 alloys exposed to (a) 0.1 $mol.L^{-1}$ Na_2SO_4 and 0.001 $mol.L^{-1}$ of NaCl solution; (b) 0.01 $mol.L^{-1}$ of NaCl solution.

In the sulfate containing solution there is indication of oxide film growth during the first hours of immersion but also oscillations of low amplitude and high frequency, behavior which is typical of attack to the oxide film by chloride ions. This was seen in both solutions showing that

even very low concentrations of chloride ions are harmful to the stability of the oxide film on Al-alloys. Lower potentials were associated to the AA2098-T351 compared to the AA2024-T3 and due to the presence of lithium in the matrix besides the lower copper content in the first alloy comparatively to the AA2024-T3, Figure 1 (a) and (b). Despite the oscillations in open circuit potential suggesting a competition between the breakdown of the passive film and its growth, fairly stable potentials were obtained from 8h onwards until the end of test (24h).

The results are in agreement with the observation of alloys surface during 24h of immersion, Figure 2 that shows that the corrosion sites were developed mainly in the first 8h of exposure to the electrolyte, for the AA2098-T351 some sites of localized corrosion were observed after the first hours of immersion (red arrows) and it was fairly stable until 24h of exposure to the solution with sulfate. A larger number of spots corresponding to pits were seen in the AA2024-T3 alloy due to the also greater number of micrometric particles.

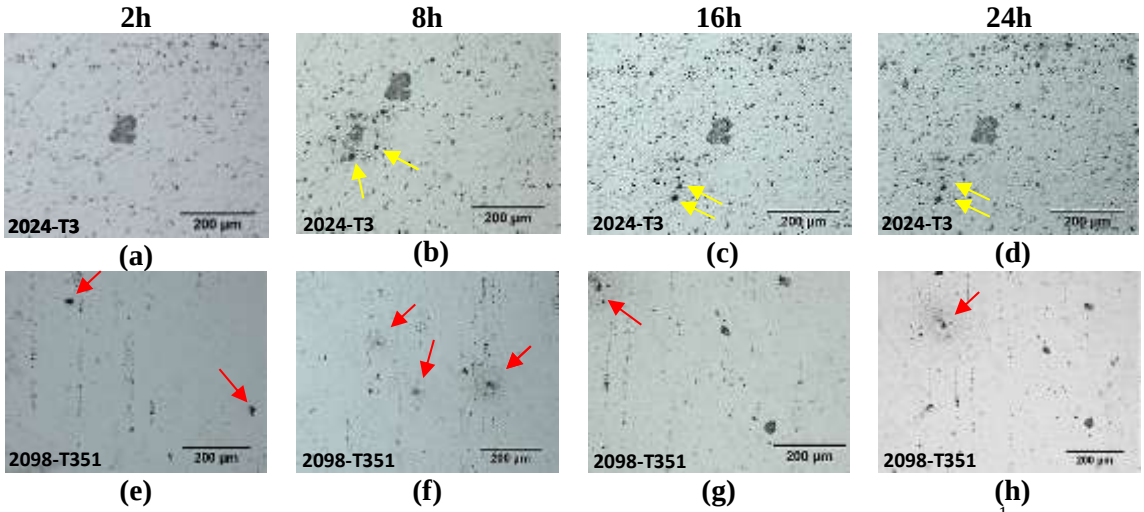

Figure 2 – Corrosion evolution of Al alloys during 24h of immersion in 0.1 mol. L^{-1} of Na_2SO_4 with 0.001 mol.L^{-1} of NaCl

Lower potentials for both alloys were measured in the chloride solution without sulfate comparatively to that with sulfate, Figure 2 and Figure 3, due to the higher aggressiveness of the first and the OCP in this solution stabilized earlier than in the sulfate containing one. This was supported by surface observation that showed development of larger pits in the AA2024-T3 alloy (yellow arrows). In the first alloy localized attack was mainly associated to the micrometric particles, but at some sites, rings of corrosion products and cathodically protected areas surrounding the pits (yellow arrows) indicated the occurrence of severe localized corrosion (SLC). In the AA2098-T351, besides pitting related to micrometric particles, SLC was also seen but it was associated to another microstructural feature and resulted in the attack of whole grains (red arrows).

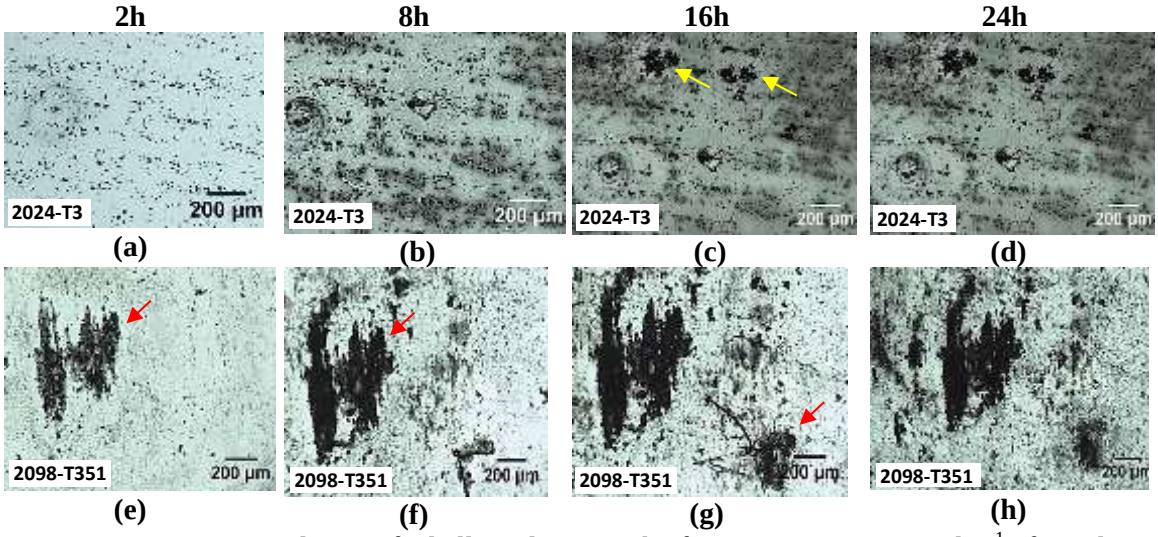

Figure 3 – Corrosion evolution of Al alloys during 24 h of immersion in 0.01 mol.L^{-1} of NaCl.

The mechanism of SLC in AA2024-T3 was reported in literature and was associated with intergranular corrosion (IGC) [36–40]. In fact, IGC was observed in the AA2024-T3 alloy, Figure 4a, whereas for the AA2098-T351, the SLC sites were related with intragranular corrosion, Figure 4b.

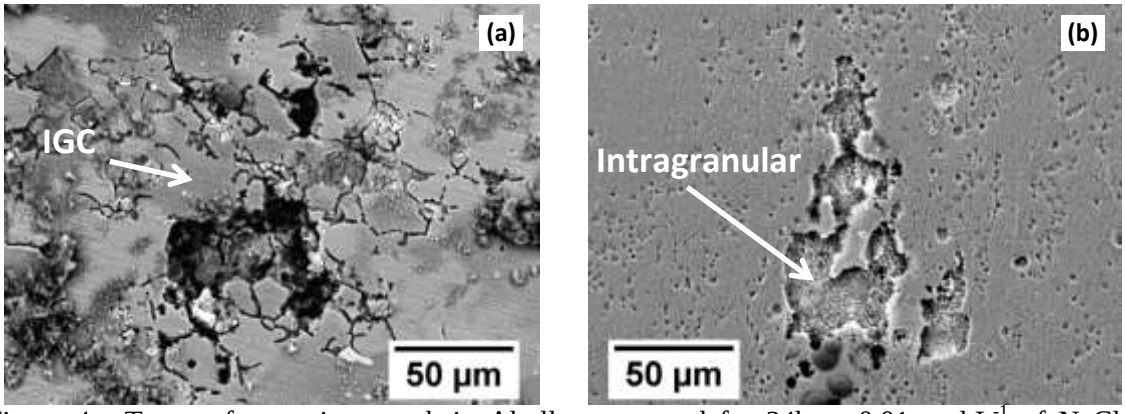

Figure 4 - Types of corrosion attack in Al-alloys exposed for 24h to 0.01 mol.L^{-1} of NaCl solution. (a) AA2024-T3; (b) AA2098-T351 alloys.

The polarization curves of both tested alloys in the two environments are shown in Figure 4. In the sulfate solution with low concentration of chloride, the anodic curves suggest that both alloys are passive. It also shows higher cathodic currents related to the AA2024-T3 alloy what is due to the larger number of cathodic micrometric particles in this alloy comparatively to the AA2098-T351. In the chloride solution without sulfate, however, both alloys are active in the corrosion potential, and the pitting potential is below the corrosion potential. Slightly lower cathodic current densities were related to the AA2098-T351 as compared with the AA2024-T3, for the same reasons presented earlier.

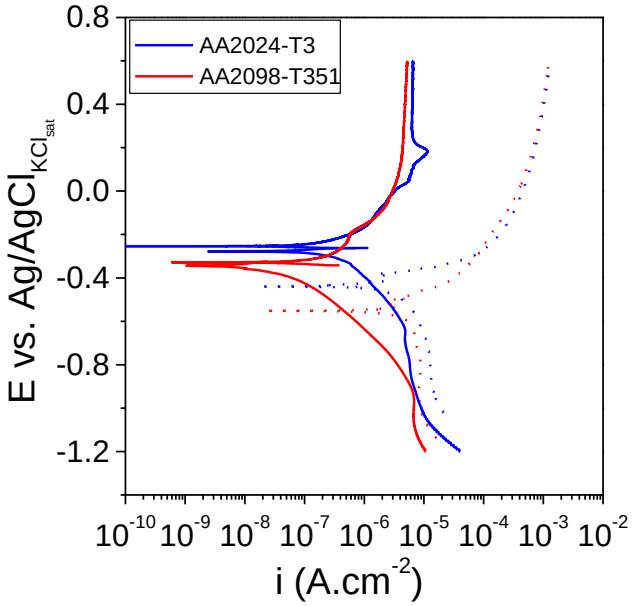

Figure 5 – Polarization curves of the AA2024-T3 and AA2098-T351 alloys after 30 min of immersion in the tested solutions used. The dashed lines correspond to results in a 0.01 mol.L^{-1} of NaCl and the solid lines to 0.1 mol.L^{-1} of Na_2SO_4 and 0.001 mol.L^{-1} of NaCl solution.

The corrosion process in both alloys in the chloride solution without sulfate is controlled by diffusion. Dissolution of micrometric particles in this alloy is responsible for the anodic currents in the polarization curves [19,41]. Ilevbare *et al.*[19] showed that the potential of the intermetallic free regions are higher than the intermetallic rich regions. In the AA2024-T3 surface the anodic S-phase particles represent 60% of the amount of micrometric particles [21] and this is responsible for the higher anodic current density values for the AA2024-T3 alloy compared to the AA2098-T351 one. Figure 6 shows that the amount of micrometric particles in the AA2024-T3 alloys is greater than in the AA2098-T351. In this last alloy, the anodic current densities are related to dissolution of T1 phase leading to intragranular attack as shown in Figure 3 (e) – (h) and Figure 4. These particles are mainly precipitated in the grains with higher degrees of deformation according to their orientation. These are the most susceptible sites to corrosion attack. In the sulfate containing one, the corrosion process is controlled by the passive film and the ohmic drop through it. The results show that the passive film was still stable on the Al-alloys after 30 minutes of exposure to the sulfate containing electrolyte.

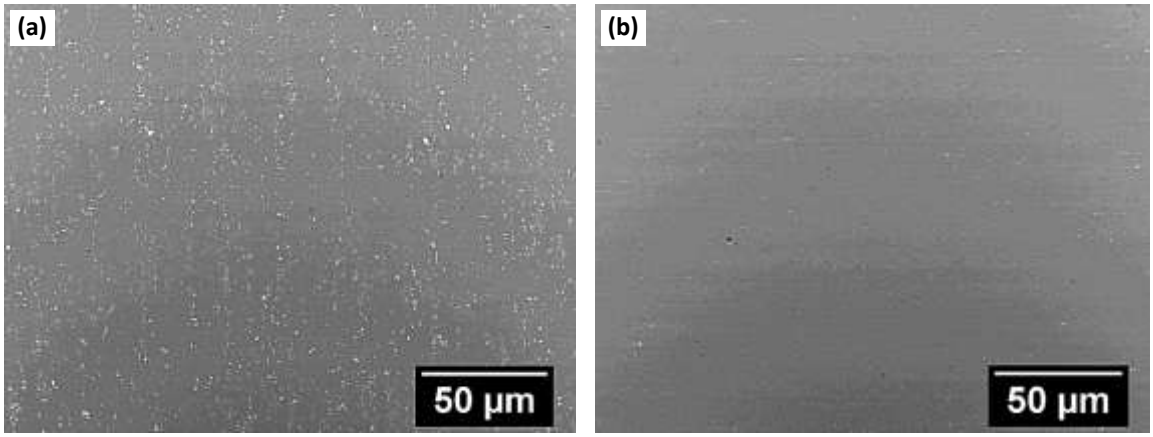

Figure 6 – SEM micrographs showing micrometric particles on the surface of the tested Al-alloys, (a) AA2024-T3; (b) AA2098-T351.

The results of EIS measurements obtained in 0.1 mol.L^{-1} of Na_2SO_4 with 0.001 mol.L^{-1} of NaCl are shown in Figure 7.

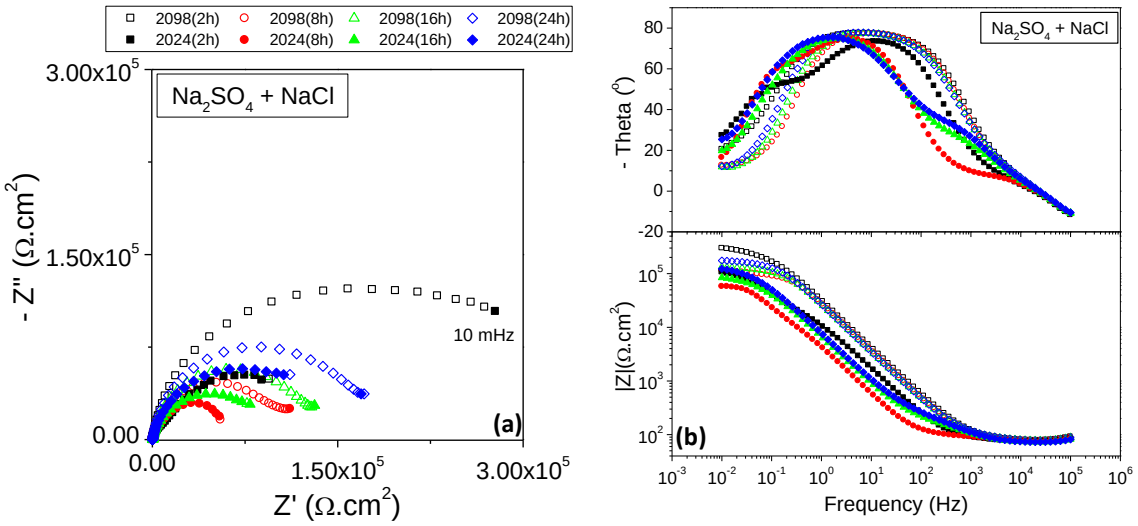

Figure 7 – EIS results for AA2024-T3 and AA2098-T351 alloys in 0.1 mol.L^{-1} of Na_2SO_4 with 0.001 mol.L^{-1} of NaCl (a) Nyquist and (b) Bode diagrams.

Figure 7 shows that for both alloys the impedance decreased from 2h to 8h and increased between 8h and 24h of exposure to the sulfate with chloride containing solution. This result shows that after the corrosion attack at the most susceptible sites at the surface, during the first 8h of test, the oxide passive film is reformed and this explains the results of surface observation shown in Figure 2. The higher impedances obtained for the AA2098-T351 is also supported by surface observation and is explained by the lower amounts of micrometric particles at the surface of this Al-Cu-Li alloy.

AJUSTAR OS DADOS DE IMPEDÂNCIA – Maurílio pedir os dados para a Mariana – Com os resultados do ajuste, discutiremos. De qualquer forma, a constante de tempo a altas frequencias deve-se ao filme óxido, enquanto a constante em frequencias menores, deve-se a fenômenos de transferência de carga nas regiões mais ativas eletroquímicamente, principalmetne na interface entre as partículas micrométricas e a matriz. O aumento da impedância com o tempo de ensiao, deve-se ao crescimento do óxido e a diminuição da cinética dos fenômenos de transferência de carga, consequentemente.

EIS results in the 0.01 mol.L^{-1} NaCl are shown in Figure 8. This figure shows different electrochemical behavior comparatively to the solution with sulfate for both tested alloys. In the chloride solution, the contribution of the oxide film is not identified, as suggested by the polarization curves; two time constants are indicated the one at medium frequencies related to charge transfer processes related to the attack at the active sites of the alloy, and the other at lower frequencies due to diffusion controlled processes, as indicated in the cathodic polarization curves, Figure 5. According to Conde and Damborenea [30] when the attack is widespread a constant related to diffusional process is present.

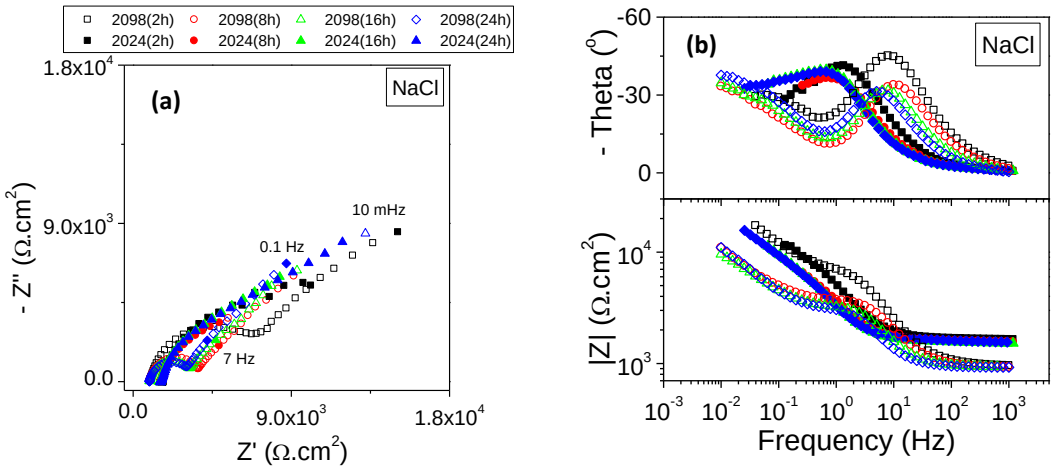

Figure 8 – (a) Nyquist and (b) Bode diagrams for the AA2024-T3 and AA2098-T351 alloys in 0.01 mol.L^{-1} of NaCl solution.

In the chloride solution, lower impedances were obtained for the AA2098-T351 than for the AA2024-T3. This result is supported by surface observation, Figure 3. This is due to the SLC found in the Al-alloys tested in this solution. It was clearly seen that the areas affected by SLC were larger in the AA2098-T351 than in the AA2024-T3 due to the presence of T1 phase in the first alloy.

Conclusions

The two Al-alloys studied in this work, AA2098-T351 and AA2024-T3, showed susceptibility to localized attack since the first hours of exposure to the electrolyte. The mechanisms of corrosion were dependent on the alloy and the electrolyte used. In the electrolyte of low aggressiveness, the AA2098-T351 showed higher resistance to localized corrosion than AA2024-T3. On the other hand, in the chloride solution, severe localized corrosion was favored in the AA2098-T351, that showed lower resistance to localized corrosion.

Acknowledgements

The authors acknowledge CAPES (Capes/Cofecub N° 806-14) and FAPESP (2013/13235-6) for financial support for this work and to CAPES for the grants of M.X. Milagre (99999.000332/2016-00), C.S.C. Machado (99999.000400/2016-05) and FAPESP for the grants of U. Donatus (Proc.2017/03095-3).

References

1. M. Mokaddem, P. Volovitch, F. Rechou, R. Oltra, and K. Ogle, *Electrochim. Acta*, **55**, 3779–3786 (2010).
2. D. Zhao, J. Sun, L. Zhang, Y. Tan, and J. Li, *J. Rare Earths*, **28**, 371–374 (2010).
3. W. G. Fahrenholtz, M. J. O 'keefe, H. Zhou, and J. T. Grant, *Surf. Coatings Technol.*, **155**, 208–213 (2002).
4. American Society for Materials, *ASM Handbook Properties and selection: Nonferrous alloys and Special-purpose Materials*, p. 3470, (2001).
5. Y. Ma et al., *Electrochim. Acta*, **80**, 148–159 (2012).
6. Y. Ma et al., *J. Electrochem. Soc.*, **158**, C17 (2011).
7. Y. Ma et al., **163**, 369–376 (2016).
8. Y. Ma et al., *Mater. Chem. Phys.*, **161**, 201–210 (2015).

9. Y. Ma et al., *Corros. Sci.*, **53**, 4141–4151 (2011).
10. Y. Ma et al., *Corros. Sci.*, **107**, 41–48 (2015).
11. C. Blanc, A. Freulon, M. C. Lafont, Y. Kihn, and G. Mankowski, *Corros. Sci.*, **48**, 3838–3851 (2006).
12. P. Campestrini, H. Terryn, A. Hovestad, and J. H. W. de Wit, *Surf. Coatings Technol.*, **176**, 365–381 (2004).
13. Z. Szklarska-Smialowska, *Coi'rosion Sci.*, **33**, 1193–1202 (1992).
14. Z. Szklarska-Smialowska, *Corros. Sci.*, **41**, 1743–1767 (1999).
15. E. Mccafferty, *Corros. Sci.*, **37**, 481–492 (1995).
16. E. McCafferty, *Corros. Sci.*, **45**, 1421–1438 (2003).
17. C. M. Liao, J. M. Olive, M. Gao, and R. P. Wei, *Corrosion*, **54**, 451–458 (1998).
18. C. Blanc, B. Lavelle, and G. Mankowski, *Corros. Sci.*, **39**, 495–510 (1997).
19. G. O. Ilevbare, O. Schneider, R. G. Kelly, and J. R. Scully, *J. Electrochem. Soc.*, **151**, 453–464 (2004).
20. F. M. Queiroz, M. Magnani, I. Costa, and H. G. de Melo, *Corros. Sci.*, **50**, 2646–2657 (2008).
21. R. G. Buchheit, *J. Electrochem. Soc.*, **144**, 2621 (1997).
22. W. Zhang and G. S. Frankel, *Electrochim. Acta*, **48**, 1193–1210 (2003).
23. X. Liu, G. S. Frankel, B. Zoofan, and S. I. Rokhlin, *Corros. Sci.*, **46**, 405–425 (2004).
24. V. Guillaumin and G. Mankowski, *Corros. Sci.*, **41**, 421–438 (1999).
25. Y. Ma, X. Zhou, G. E. Thompson, and P. Skeldon, *Corros. Sci.*, **66**, 292–299 (2013).
26. U. Donatus et al., *Corros. Sci.* (2017).
27. J. V. de Sousa Araujo et al., *Corros. Sci.*, **133**, 132–140 (2018).
28. G. E. S. R.G. Buchheit Jr., J.P. Moran, *Corrosion*, **46**, 610–617 (1990).
29. M. Guérin et al., *Corros. Sci.*, **102**, 291–300 (2016).
30. A. Conde and J. De Damborenea, *Corros. Sci.*, **39**, 295–303 (1997).
31. J. Ryl et al., *Corros. Sci.*, **87**, 150–155 (2014)
32. C. Luo et al., *J. Alloys Compd.*, **658**, 61–70 (2016)
33. W. N. Garrard, *Corros. Sci.*, **50**, 215–225 (1994).
34. X. Yue, W. Xiaojing, Y. Zhaotong, and L. Jiaxue, *Chinese J. Aeronaut.*, **24**, 681–686 (2011).
35. M. Guérin, E. Andrieu, G. Odemer, J. Alexis, and C. Blanc, *Corros. Sci.*, **85**, 455–470 (2014).
36. A. Boag et al., *Corros. Sci.*, **52**, 90–103 (2010).
37. A. E. Hughes et al., in *Recent Trends in Processing and Degradation of Aluminium Alloys*,, p. 223–262, InTech (2011).
38. A. E. Hughes et al., *Corros. Sci.*, **53**, 27–39 (2011).
39. A. Boag, A. E. Hughes, A. M. Glenn, T. H. Muster, and D. McCulloch, *Corros. Sci.*, **53**, 17–26 (2011).
40. A. M. Glenn et al., *Corros. Sci.*, **53**, 40–50 (2011) .
41. T. M. D. C. Kumai, J. Kusinski, G. Thomas, C. Kumai, J. Kusinski, G. Thomas, and T. M. Devine, *Corros. Sci.*, **45**, 294–302 (1989).